Zinc Clusters

International Edition: DOI: 10.1002/anie.201510762
German Edition: DOI: 10.1002/ange.201510762

Atom-Precise Organometallic Zinc Clusters

Hung Banh, Katharina Dilchert, Christine Schulz, Christian Gemel, Rüdiger W. Seidel, Régis Gautier, Samia Kahlal, Jean-Yves Saillard, and Roland A. Fischer**

Abstract: *The bottom-up synthesis of organometallic zinc clusters is described. The cation {[Zn$_{10}$](Cp*)$_6$Me}$^+$ (**1**) is obtained by reacting [Zn$_2$Cp*$_2$] with [FeCp$_2$][BAr$_4^F$] in the presence of ZnMe$_2$. In the presence of suitable ligands, the high reactivity of **1** enables the controlled abstraction of single Zn units, providing access to the lower-nuclearity clusters {[Zn$_9$](Cp*)$_6$} (**2**) and {[Zn$_8$](Cp*)$_5$(^{t}BuNC)$_3$}$^+$ (**3**). According to DFT calculations, **1** and **2** can be described as closed-shell species that are electron-deficient in terms of the Wade–Mingos rules because the apical ZnCp* units that constitute the cluster cage do not have three, but only one, frontier orbitals available for cluster bonding. Zinc behaves flexibly in building the skeletal metal–metal bonds, sometimes providing one major frontier orbital (like Group 11 metals) and sometimes providing three frontier orbitals (like Group 13 elements).*

Quantum-chemical calculations have shown that naked metalloid zinc clusters Zn$_a$ ($a > 8$) have a large spectrum of electronic properties, ranging from a metallic to an insulating character, and may also show special features that uniquely combine both phenomena.[1] Ligand-protected metal clusters [M$_a$](L)$_b$ ($a > b$), linking molecular and bulk materials, have been the focus of research for a long time. Zinc, however, has remained an exception. Naked Zn clusters have only been studied in the gas phase,[1] as a guest in Zeolite X,[2] or as discrete structural units in intermetallic frameworks[3] and porous materials.[4] The closed-shell electron configuration of Zn only allows for weak van der Waals interactions in small homoleptic clusters.[5] Stabilization by the effective mixing of s/p states requires larger nuclearities.[1] Notably, our series of compounds, [M@Zn$_a$](L)$_a$ (M = d block metal, L = Cp* (Cp* = pentamethylcyclopentadienyl), CH$_3$; a = 8–12), represents examples of Zn-rich cluster-like molecules.[6] However, the "empty" [Zn$_a$](L)$_a$ cages are not stable without the strong binding to the interstitial metal M, for example, in [Mo@Zn$_{12}$](Cp*)$_3$(Me)$_9$. Ligand-protected molecular Zn clusters [Zn$_a$](L)$_b$ have not been reported to date.

[*] H. Banh, K. Dilchert, C. Schulz, Dr. C. Gemel, Dr. R. W. Seidel, Prof. Dr. R. A. Fischer
Anorganische Chemie II - Organometallics and Materials
Fakultät für Chemie und Biochemie
Ruhr-Universität Bochum
44780 Bochum (Germany)
E-mail: roland.fischer@rub.de
Dr. R. Gautier, Dr. S. Kahlal, Prof. Dr. J.-Y. Saillard
Institut des Sciences Chimiques de Rennes
UMR 6226 CNRS-ENSC Rennes, Université de Rennes 1
35042 Rennes Cedex (France)
E-mail: jean-yves.saillard@univ-rennes1.fr

Supporting information for this article is available on the WWW under http://dx.doi.org/10.1002/anie.201510762.

Recently, Jones and co-workers employed the bulky amido ligand L$_N$ (L$_N$ = N(Ar)SiMe$_3$, Ar = 2,6-{C(H)Ph$_2$}$_2$-4-^{i}Pr-C$_6$H$_2$) to stabilize the mixed-valance three-membered zinc chain [L$_N$ZnZnZnL$_N$].[7] On the one hand, the bulkiness of L$_N$ supports the unique linear structure of the [Zn$_3$] unit, but on the other hand, it reduces the flexibility of coordination modes and the reactivity at the Zn atoms. This is different for the trigonal cluster cation {[Zn$_3$](Cp*)$_3$}$^+$, which becomes important in this context.[8] It was obtained by the addition of the in situ formed solvated cation [ZnCp*]$^+$ to Carmona's compound, [Zn$_2$Cp*$_2$] = [Zn$_2$](Cp*)$_2$. Regarded as a minimal building unit of larger deltahedral Zn-containing clusters, it points towards the accessibility of [Zn$_a$]L$_b$ below the critical size limit for naked jellium super-atom-like Zn clusters. Interestingly, gallium, as the right neighbor of Zn in the periodic table, features a rich metalloid cluster chemistry, and the same is true for Al, the lighter homologue. A library of anionic {[M$_a$]L$_b$}$^{n-}$ (M = Al, Ga; $a > b$; L = N(SiMe$_3$)$_2$) complexes were previously obtained and thoroughly studied.[9] The key to this bottom-up wet chemical synthesis of metalloid clusters is the controlled disproportionation of the metastable monohalides MX in solution at low temperatures and the trapping of intermediates by the addition of a judiciously chosen ligand L.

Inspired by Schnöckel's pioneering work cited above, we have been exploring the transfer of this reaction concept to ligand-protected Zn clusters using [Zn$_2$](Cp*)$_2$ as the primary Zn source and considering the Cp* group as a removable protecting group. Notably, semi-deprotected [Cp*Zn$_2$-(Et$_2$O)$_3$]$^+$ can be isolated at room temperature by oxidative cleavage of one Zn–Cp* bond and is prone to disproportionation.[10] This species can be used as a Zn source, and the reactivity of {[Cp*Zn$_2$](L′$_n$)}$^+$ can be modulated by the choice of solvent or weakly coordinating co-ligands L′. However, as [Cp*Zn$_2$]$^+$ cannot be isolated without unwanted stabilization, we explored its in situ activation by the single-electron oxidation of one Zn–Cp* bond (with formation of the by-product Cp*$_2$, decamethylfulvalene). The addition of small quantities of ZnMe$_2$ proved to be crucial as it acts as a methyl-transfer and/or -trapping reagent. Accordingly (Scheme 1), we obtained the first all-hydrocarbon-ligand-protected medium-nuclearity clusters [Zn$_a$]L$_b$ **1**–**3** (Figure 1).

The reaction of [Zn$_2$](Cp*)$_2$ with [FeCp$_2$][BAr$_4^F$] (BAr$_4^F$ = B{C$_6$H$_3$(CF$_3$)$_2$}$_4$) and ZnMe$_2$ (12:2:1 molar ratio) in fluorobenzene (C$_6$H$_5$F) at −30 °C leads to the formation of the salt {[Zn$_{10}$](Cp*)$_6$Me}[BAr$_4^F$] (**1**[BAr$_4^F$]) as red microcrystals and their isolation in 41 % yield (based on Zn). The overall reaction involves an oxidative Zn–Cp* bond cleavage by [FeCp$_2$][BAr$_4^F$]. The by-products [FeCp$_2$], Cp*$_2$, and Cp*$_2$Zn were identified by in situ NMR spectroscopy. However, when [Zn$_2$Cp*$_2$] is treated with [FeCp$_2$][BAr$_4^F$] in the absence of

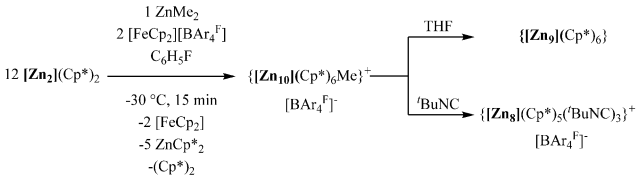

Scheme 1. Synthesis of the first examples of medium-size ligand-protected Zn clusters: $\{[Zn_{10}](Cp^*)_6Me\}^+$ (**1**), $\{[Zn_9](Cp^*)_6\}$ (**2**), and $\{[Zn_8](Cp^*)_5(^t\text{BuNC})_3\}^+$ (**3**).

$ZnMe_2$ under otherwise identical conditions, no reaction takes place. Based on these observations, we draw the (conceptual) conclusion that the in situ formation of the dimeric intermediate Zn^I species [RZn–ZnMe] (R = Me or Cp*), which involves rapid Me/Cp* group exchange, may lead to Zn^0 upon disproportionation, which is then stabilized by the abundant ·ZnCp* radicals.

Compound **1**$[BAr_4^F]$ is soluble in non-coordinating, polar, aprotic solvents, such as C_6H_5F or CH_2Cl_2, under strict exclusion of moisture. Without continuous cooling to −10 °C, however, it rapidly decomposes in solution as well as in the solid state. The elemental analysis (C, H) and AAS (Zn) data are in reasonable agreement with the assigned composition, in particular considering its very high sensitivity, which impedes storage and sample transfer. Accordingly, the ^{1}H NMR data (CD_2Cl_2, 25 °C) reveal thus far unidentified decomposition products, including CH_4 ($\delta = 0.21$ ppm). NMR spectra recorded at −90 °C (isolated, pure sample) are clean and show one singlet at 0.02 ppm (s, 3H, Zn–CH_3) and one singlet at 1.75 ppm (s, 30H, μ_4-ZnCp* groups). Another two, not fully decoalesced singlets are assigned to terminal and edge-bridging (μ_2) ZnCp* groups ($\delta = 2.04$, 2.06 ppm, 60H), indicating rapid fluxional behavior in the equatorial plane of **1** (Figure 1). Expectedly, a set of signals for the $[BAr_4^F]^-$ anion (7.53 ppm, 4H; 7.72 ppm, 8H) was also observed.

The lability of **1**$[BAr_4^F]$ suggests further transformations, namely cluster expansion or degradation. We investigated the reactivity of **1**$[BAr_4^F]$ towards solvents with hard σ-donor properties, such as THF or Et_2O (L), at −80 °C. In fact, selective abstraction of $[MeZn(L)_3][BAr_4^F]$ occurred, and the neutral cluster $[Zn_9](Cp^*)_6$ (**2**) was obtained. One single framework Zn atom is selectively excised as the cationic $[MeZn(L)_3]^+$ adduct, that is, as a Zn^{II} species. The triangular cation $\{[Zn_3](Cp^*_3)\}^+$ shows a similar behavior. It is selectively fragmented into $[Zn_2Cp^*_2]$ and $[Cp^*Zn(THF)_3]^+$ upon addition of THF.[8b] The neutral Zn_9 cluster **2** is soluble and stable in both coordinating and non-coordinating solvents. However, like **1**$[BAr_4^F]$, it needs to be handled with great care with rigorous air and moisture exclusion, and continuous cooling is needed to avoid or reduce decomposition. Slow diffusion of *n*-pentane into a concentrated toluene solution at −90 °C afforded single crystals of **2**·2 toluene. The NMR spectrum (CD_2Cl_2) at −90 °C shows two resonances at 1.87 (s, 30H) and 1.97 ppm (s, 60H) in a 1:2 ratio although decoalescence is still not complete, indicating the high fluxionality of all Cp* groups. The signals at 2.27 (s, 6H) and 7.05–7.27 ppm (m, 10H) are due to toluene solvate molecules incorporated into the single crystals.

The controlled deconstruction of the cationic Zn_{10} cluster **1** using ^{t}BuNC as a somewhat softer ligand (−30 °C, C_6H_5F) gives the Zn_8 cluster **3** as the salt $\{[Zn_8](Cp^*)_5(^t\text{BuNC})_3\}$-$[BAr_4^F]$. The by-products have not been identified yet. Yellow single crystals of **3**$[BAr_4^F]\cdot 4FC_6H_5$ (monoclinic, *C*2/*c*, eight formula units in the unit cell) were obtained by slow diffusion of *n*-hexane into the reaction solution at −30 °C.[11] The molecular structure consists of two corner-connected Zn_4 rhombi (flipped by ca. 90°) with one additional terminal ZnCp* ligand at Zn7 (Figure 1). The bridging Zn atoms feature Cp* ligands, and the open sites (Zn1, Zn7) at the corners of the Zn_4 rhombi are saturated by ^{t}BuNC.

Knowledge of the controlled removal of ZnR groups from hetero- as well as homonuclear Zn clusters or their substitution by organic ligands is rather limited. However, as shown above, controlled deconstruction is possible. With a hard donor, such as THF or diethyl ether (L), one Zn atom is removed from the $[Zn_{10}]$ structure in the form of the rather hard acid–base adduct $[MeZn^{II}(L)_3]^+$. The use of the softer ^{t}BuNC ligand, however, leads to direct coordination at the cluster core and the subsequent ejection of labile ZnR species. These results are in accordance with our previous studies on the reactivity of $[Zn_2(THF)_6][BAr_4^F]_2$ towards isonitriles, where the higher affinity of the soft RNC ligands (R = ^{t}Bu or Ph) enabled the facile substitution of the THF molecules by isonitriles at the Zn centers.[12]

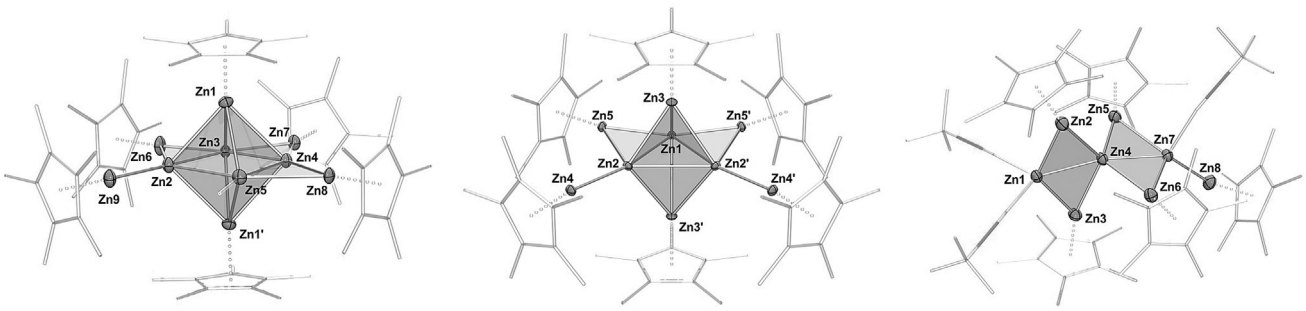

Figure 1. Zinc cores of the ligand-protected clusters $\{[Zn_{10}](Cp^*)_6Me\}^+$ (left), $\{[Zn_9](Cp^*)_6\}$ (middle), and $\{[Zn_8](Cp^*)_5(^t\text{BuNC})_3\}^+$ (right). Thermal ellipsoids set at 50% probability. Symmetry-related atoms are indicated by ′. All clusters feature Zn_3 triangles as a structural motif. For details on the crystallographic data collection, structural parameters, and further discussion, see the Supporting information.

The solvate **1**$[BAr_4^F]\cdot 5FC_6H_5$, which was obtained from a concentrated C_6H_5F solution at −30 °C (monoclinic, *Pm*, one formula unit in the unit cell), was analyzed by single-crystal X-ray diffraction. The packing reveals alternating sheets of $[Zn_{10}]^+$ clusters and $[BAr_4^F]^-$ anions. The structure of **1** (Figure 1) resembles a rather symmetric Zn_6 octahedron with three edge-bridging ZnCp*, one terminal ZnCp*, and one CH_3 group (see the Supporting Information, Figure S5). The equatorial Zn atoms of the core (Zn2–Zn5) are coplanar with the bridging and terminal Zn atoms. Interestingly, there is an elongated edge in the equatorial plane. The Zn2–Zn5 distance (2.833(3) Å) is elongated compared to the other three edges capped by ZnCp* (Zn3–Zn4 2.425(2); Zn2–Zn3 2.456(2) Å). As there are only few molecular Zn-containing clusters, the anionic intermetallic cluster $[Zn_{cen}@(Zn_8Bi_4)_{ico}@Bi_7]_5^-$ may be useful for comparison here.[13] It shows that the longer Zn2–Zn5 distance of **1** is well in the range of binding Zn_{cen}–Zn_{ico} contacts (2.832(2)–2.859(3) Å; see the Supporting Information).

Yellow crystals of **2**·THF (orthorhombic, *Cmcm*, four molecules in the unit cell) were obtained by slow diffusion of *n*-hexane into the reaction solution at −30 °C. The molecular structure of **2** (Figures 1, S6) features a distorted trigonal-bipyramidal Zn_5 core whose equatorial plane (Zn1, Zn2, Zn2′) contains two edge-bridging and two terminal ZnCp* units. This structure can be derived by removing the ZnMe group (Zn5) from **1** and forming a bond between Zn2 and Zn4 (Figure 2). The resulting structure of **2** exhibits an elongated edge (Zn2–Zn2′ 2.829(8) Å) without a bridging ZnCp* group. Another similarity to **1** is the plane spanned by the edge-bridging ZnCp* ligands and the equatorial Zn atoms. However, **2** appears to be more contracted within the equatorial plane as a result of the removal of the ZnMe group, and accordingly, it is slightly expanded in the orthogonal direction (Figure 2). The position of the apical μ_3-ZnCp* group (Zn3 or Zn3′) of **2** is a bit farther from the equatorial plane (distance 2.137 Å) than the respective position of the apical μ_4-ZnCp* group (Zn1 or Zn1′) of **1**, with a shorter distance of 2.008 Å.

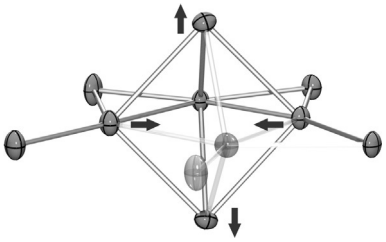

Figure 2. Relation of the Zn cores of **1** and **2**. Contraction and expansion from $[Zn_{10}]$ to $[Zn_9]$ is indicated by arrows. Cleaved bonds and removed atoms are transparent.

DFT calculations at the Def2TZVP/PBE0 level of theory (see the Supporting Information) were carried out on **1** and **2** as well as their hypothetical relatives, cationic $\{[Zn_{10}](Cp)_6Me\}^+$ (**1′**) and neutral $[Zn_9](Cp)_6$ (**2′**), which both bear C_5H_5 ligands (Cp rather than Cp*). The optimized structures of **1**, **1′** and **2**, **2′** are in a fairly good agreement with the X-ray structures (see above, Table S3). This includes the long unsupported Zn–Zn contact, which was computed to be 2.833 Å for **1** and 2.573 Å for **1′** (expected value for **1**: 2.832(2) Å). The respective values are 3.066 Å for **2** and 2.804 Å for **2′** (expected value for **2**: 2.829(8) Å). The computed HOMO–LUMO gaps (**1**: 3.20 eV; **2**: 3.86 eV) are indicative of a closed-shell structure and consistent with the (relative) kinetic stability of the clusters.

Looking first at **1**, its octahedral Zn_6 core can be fragmented into two axial μ_4-ZnCp* units, two Zn−R units (Zn−Me and Zn−ZnCp*), and two Zn atoms. Furthermore, there are three edge-bridging μ_2-ZnCp* fragments. Each ZnCp* and Zn−R unit provides one electron, whereas each Zn atom contributes two electrons. Taking the charge of the cationic cluster into account, one ends up with five skeletal electron pairs (SEPs) that are available for Zn–Zn bonding within the whole edged-bridged octahedral core. The Wade–Mingos electron-counting rules[14] predict a total of seven SEPs for a regular octahedral cluster such as $[B_6H_6]^{2-}$, for example. To understand the four-electron discrepancy, it is important to consider that these particular rules apply only to clusters made of fragments that possess three frontier orbitals (one σ-type and two π-type).[14c,d] This is the case with BH, for example, as well as for a Zn−R unit or a bare Zn atom. However, this is not the case for a ZnCp* fragment. With only one singly occupied σ-type frontier orbital, ZnCp* is isolobal to H. "Deprotonating" **1** by formally removing the three edge-bridging $[ZnCp^*]^+$ units leads to the hypothetical octahedral $\{Zn_6Cp^*_2RR'\}^{2-}$ (R = Me, R′ = ZnCp*) system.

The seven SEPs of $[B_6H_6]^{2-}$ correspond to the $(a_{1g})^2(t_{2g})^6(t_{1u})^6$ configuration. Whereas the skeletal-bonding a_{1g} MO is a pure σ-type combination, and the t_{1u} MOs are of mixed σ and π origin, the t_{2g} MOs are pure π-type combinations. Considering the octahedron edges as three interpenetrating squares, each t_{2g} component can be associated with one of the squares (Scheme 2, left). In the case of **1**, as the two apical ZnCp* fragments have no π-type frontier orbitals, one is left with two "t_{2g}-derived" components lacking apical contributions (the black and blue squares; the one associated with the black square is shown on the right side of Scheme 2). Therefore, these two components are not strongly bonding as in $[B_6H_6]^{2-}$. Rather, they are non-bonding and of high energy owing to their 4p(Zn) character. As a consequence, they are not available to electrons, and the closed-shell configuration of **1** corresponds to five rather than seven SEPs, as would be expected for Wade–Mingos-type clusters. Another and an equivalent way to understand this peculiar electron count is to consider the fully "deprotonated"

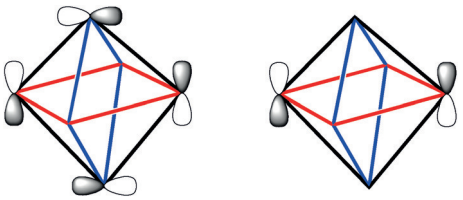

Scheme 2. Left: One of the occupied t_{2g} skeletal orbitals in $[B_6H_6]^{2-}$. Right: The related t_{2g}-derived orbital lacking π-type contributions from the apical positions as in **1**.

$\{Zn_4RR'\}^{4-}$ (R = Me, R′ = ZnCp*) planar system, with four bonding electron pairs associated with four localized Zn–Zn σ bonds and the fifth pair in an in-phase fully π-type bonding orbital. This makes the Zn–Zn bonding in $\{Zn_4RR'\}^{4-}$ equivalent to the C–C bonding in the planar cyclobutadiene dication, $\{C_4H_4\}^{2+}$. In the $\{Zn_6Cp^*_2RR'\}^{2-}$ octahedral system, the π-type bonding orbital is strongly stabilized by the out-of-phase combination of the two σ-type orbitals on the two apical ZnCp* fragments. Of course, the five SEPs are not only associated with the bonding along the twelve octahedron edges, but also with the bonding between the three μ_2-ZnCp* units and the octahedron. This is one of the reasons, aside from the template edge-bridging effect, for the shorter bridged edges of the octahedron compared to the weaker unbridged one. As the low symmetry of **1** and **1′** allows for substantial mixing, it is not possible to clearly identify five major occupied Kohn–Sham MOs associated with their five SEPs. However, it is easier in the isoelectronic and isostructural model $\{[Zn]_9(Cp)_5Me_2\}^+$ (**1″**) of C_{2v} symmetry (Figure 3). Model **1″** is derived from **1′** by replacing the terminal ZnCp unit by CH_3 (unsupported Zn–Zn bond: 2.783 Å).

The same procedure as for **1** can be applied to understand the electron count of **2**, which can be reformulated as $\{Zn_7Cp^*_4R_2\}$ (R = ZnCp*). The "deprotonated" hypothetical $\{Zn_5Cp^*_2R_2\}^{2-}$ triangular bipyramid is a species with four SEPs whereas the Wade–Mingos rules predict six SEPs.[14b,c] The discrepancy is, as for **1**, related to the lack of π-type frontier orbitals on the ZnCp* apices, which in turn causes the absence of two low-lying skeletal MOs of e″ symmetry. Alternatively, three of the four SEPs can be associated with σ-type bonding Zn–Zn electron pairs along the equatorial triangle; the fourth one occupies the in-phase fully bonding π-type combination on the same triangle, which is additionally stabilized by the out-of-phase combination of the σ-type orbitals of the two apical ZnCp* fragments. Again, the electron deficiency and large delocalization in **2** cause the unbridged Zn–Zn edge to be weaker. The four occupied MOs that most accurately represent the four delocalized SEPs in **2′** are shown in Figure S13.

The strengths of the long, unsupported Zn–Zn bonds in **1** and **2** can be addressed in various ways. The Wiberg indices associated with these bonds, computed with the NBO 5.0 program,[15] are 0.06 and 0.05 for **1′** and **2′**, respectively (similar values were found for **1** and **2** using a slightly contracted basis set). For comparison, the average values corresponding to the equatorial bridged bonds are 0.11 and 0.07 for **1′** and **2′**, respectively. The natural atomic orbital overlap-weighted bond indices are 0.21 for the unsupported Zn–Zn bonds in both **1′** and **2′**. Those of their corresponding bridged counterparts are 0.36 and 0.30, respectively. Complementary insight into the nature of the bonding is provided in Figure 4, which shows the electron localization function (ELF)[16] density of a slice through the Zn2–Zn9 plane for cluster **1′**. Considering the Zn–Zn contacts, larger ELF densities (signifying localization) are mostly found for the center of the Zn_3 triangles that result from the capping of the octahedron edges, as well as at the center of the Zn2-Zn5-Zn9 triangle. The ELF topology (Figure 4) does not discriminate the elongated Zn2–Zn5 bond from the other Zn–Zn contacts of the capped octahedron. Clearly, all of these data support the hypothesis that significant bonding exists along the equatorial unsupported edge of clusters **1** and **2**. This is consistent with the overall electron deficiency of these compounds in which zinc behaves flexibly in building skeletal metal–metal bonds, sometimes using one major frontier

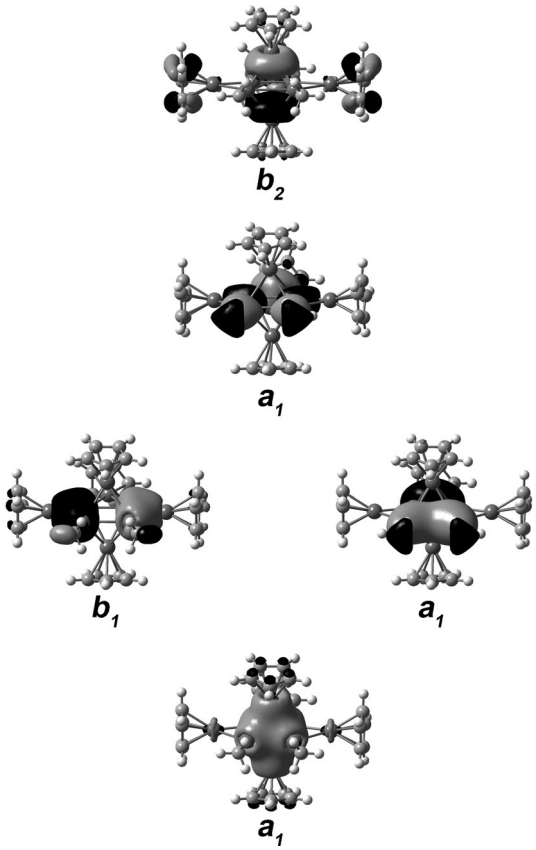

Figure 3. The major Kohn–Sham orbitals of the model cluster $\{[Zn]_9(Cp)_5Me_2\}^+$ (**1″**, C_{2v}) associated with the five SEPs.

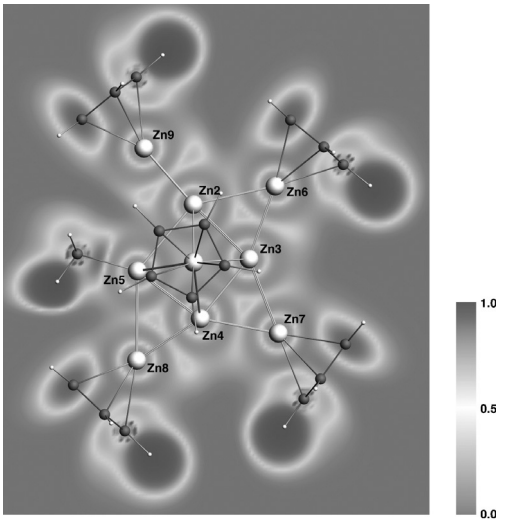

Figure 4. ELF color density plot of a slice through the Zn2–Zn9 plane in the cation $\{[Zn_{10}](Cp^*_6Me)\}^+$ (**1′**).

orbital (like Group 11 metals) and sometimes using three frontier orbitals (like Group 13 elements).

Lastly, let us look back to the title of this paper: At first glance, "atom-precise clusters" seems redundant. With the results of the computational studies in mind, the term "cluster" strictly refers to the skeletal cluster cores of the presented compounds. For Zn_{10} cluster **1**, for example, the core consists of six rather than ten zinc atoms. However, the electronic structure of this core requires four more zinc atoms that act as "ligands" to provide the exact number of skeletal electrons necessary for stabilizing the octahedral core structure. "Atom-precise" in this context does therefore not only refer to an exactly defined, denumerable number of atoms but rather denotes an "exact number of metal atoms required for the stabilization of deltahedral cluster core structures consistent with the Wade–Mingos rules".

In summary, clusters **1**, **2**, **3**, and $\{[Zn_3](Cp^*)_3\}^+$ are the first examples of ligand-protected deltahedral Zn clusters. The controlled disproportionation of metastable organometallic Zn^I species with removable protecting ligands is key to access these structures. The new clusters are electron-deficient (Wade–Mingos rules), which is due to the lack of π-type frontier orbitals on the ZnCp* moieties, which are isolobal to H rather than to BH. The comparatively weak skeletal bonding suggests a rich chemistry and the existence of other and larger atom-precise $[Zn_a]$ clusters, which could be obtained by varying the reaction partners, conditions, and stabilizing ligands. We also anticipate **1** and **2** to be precursors for Hume–Rothery-type intermetallic clusters. For example, the reaction of **1**$[BAr_4^F]$ with $[CpCu(CN^tBu)]$ yields $\{[Cu_3Zn_5](Cp^*)_4(CN^tBu)_4\}^+$ (Figure S8), which is isostructural and isoelectronic to $[Cu_4Zn_4](Cp^*)_4(CN^tBu)_4$.[17] A further extension to mimic complex alloy structures remains a fascinating target for us. Can more complex molecular cutouts be obtained, for example, from zinc-rich quasicrystalline phases such as Zn_6Sc?[18]

Acknowledgements

This work was supported by the Deutsche Forschungsgemeinschaft (Fi-502/23-2). H.B. is grateful for a fellowship from the German Chemical Industry Fund. The GENCI is thanked for HPC resources (2015-087367).

Keywords: clusters · density functional calculations · ELF · Wade–Mingos rules · zinc

How to cite: *Angew. Chem. Int. Ed.* **2016**, *55*, 3285–3289
Angew. Chem. **2016**, *128*, 3344–3349

[1] A. Aguado, A. Vega, A. Lebon, B. von Issendorff, *Angew. Chem. Int. Ed.* **2015**, *54*, 2111–2115; *Angew. Chem.* **2015**, *127*, 2139–2143.
[2] S. Zhen, D. Bae, K. Seff, *J. Phys. Chem. B* **2000**, *104*, 515–525.
[3] a) U. Häußermann, P. Viklund, C. Svensson, S. Eriksson, P. Berastegui, S. Lidin, *Angew. Chem. Int. Ed.* **1999**, *38*, 488–492; *Angew. Chem.* **1999**, *111*, 580–584; b) P. Viklund, C. Svensson, S. Hull, S. I. Simak, P. Berastegui, U. Häußermann, *Chem. Eur. J.* **2001**, *7*, 5143–5152.
[4] P. Cui, H.-S. Hu, B. Zhao, J. T. Miller, P. Cheng, J. Li, *Nat. Commun.* **2015**, *6*, 6331.
[5] H. J. Flad, F. Schautz, Y. Wang, M. Dolg, A. Savin, *Eur. Phys. J. D* **1999**, *6*, 243–254.
[6] T. Cadenbach, T. Bollermann, C. Gemel, M. Tombul, I. Fernandez, M. von Hopffgarten, G. Frenking, R. A. Fischer, *J. Am. Chem. Soc.* **2009**, *131*, 16063–16077.
[7] J. Hicks, E. J. Underhill, C. E. Kefalidis, L. Maron, C. Jones, *Angew. Chem. Int. Ed.* **2015**, *54*, 10000–10004; *Angew. Chem.* **2015**, *127*, 10138–10142.
[8] a) I. Resa, E. Carmona, E. Gutierrez-Puebla, A. Monge, *Science* **2004**, *305*, 1136–1138; b) K. Freitag, C. Gemel, P. Jerabek, I. M. Oppel, R. W. Seidel, G. Frenking, H. Banh, K. Dilchert, R. A. Fischer, *Angew. Chem. Int. Ed.* **2015**, *54*, 4370–4374; *Angew. Chem.* **2015**, *127*, 4445–4449.
[9] H. Schnöckel, *Dalton Trans.* **2008**, 4344–4362.
[10] K. Freitag, H. Banh, C. Ganesamoorthy, C. Gemel, R. W. Seidel, R. A. Fischer, *Dalton Trans.* **2013**, *42*, 10540–10544.
[11] Compound **3** was isolated and separated from by-products by picking individual single crystals in perfluoropolyether using an optical microscope. The crystals are highly labile and rapidly decompose even at room temperature, which prevents the isolation of substantial amounts of **3** for spectroscopic or elemental analyses.
[12] H. Banh, C. Gemel, R. W. Seidel, R. A. Fischer, *Chem. Commun.* **2015**, *51*, 2170–2172.
[13] J. M. Goicoechea, S. C. Sevov, *Angew. Chem. Int. Ed.* **2006**, *45*, 5147–5150; *Angew. Chem.* **2006**, *118*, 5271–5274.
[14] a) K. Wade, *J. Chem. Soc. D* **1971**, 792–793; b) D. M. P. Mingos, *Nature Phys. Sci.* **1972**, *236*, 99–102; c) K. Wade in *Transition Metal Clusters* (Ed.: B. F. G. Johnhson), Wiley, Chichester, **1980**, pp. 193–264; d) D. M. P. Mingos in *Introduction to Cluster Chemistry*, Prentice-Hall, Englewood Cliffs, **1990**.
[15] E. D. Glendening, J. K. Badenhoop, A. E. Reed, J. E. Carpenter, J. A. Bohmann, C. M. Morales, F. Weinhold, Theoretical Chemistry Institute, University of Wisconsin, Madison, WI, **2001**, http://www.chem.wisc.edu/~nbo5.
[16] a) A. D. Becke, K. E. Edgecombe, *J. Chem. Phys.* **1990**, *92*, 5397–5403; b) M. Kohout, A. Savin, *Int. J. Quantum Chem.* **1996**, *60*, 875–882; c) U. Häußermann, S. Wengert, P. Hofmann, A. Savin, O. Jepsen, R. Nesper, *Angew. Chem. Int. Ed. Engl.* **1994**, *33*, 2069–2073; *Angew. Chem.* **1994**, *106*, 2147–2150.
[17] K. Freitag, H. Banh, C. Gemel, R. W. Seidel, S. Kahla, J.-Y. Saillard, R. A. Fischer, *Chem. Commun.* **2014**, *50*, 8681–8684.
[18] a) Y. Kaneko, Y. Arichika, T. Ishimasa, *Philos. Mag. Lett.* **2001**, *81*, 777–787; b) H. Euchner, T. Yamada, S. Rols, T. Ishimasa, J. Ollivier, H. Schober, M. Mihalkovic, M. de Boissieu, *J. Phys. Condens. Matter* **2014**, *26*, 055402.

Received: November 20, 2015
Revised: December 28, 2015
Published online: February 5, 2016

